UDC 621.45.035.01:621.794.4 **doi: 10.32620/reks.2025.4.04**

Oleksandr SHORINOV[1], Sergii POLYVIANY[2], Nina SAVCHENKO[1], Roman IPATOV[1]

[1] National Aerospace University «Kharkiv Aviation Institute», Kharkiv, Ukraine,
[2] «Motor Sich» JSC, Zaporizhzhia, Ukraine

METHODOLOGY FOR VALIDATION OF ANALYTICAL MODELS OF TWO-PHASE FLOWS IN SUPERSONIC NOZZLES USING CFD SIMULATION

*The **subject matter** of this article is the methodology for mathematical modeling of gas-dynamic processes in supersonic converging-diverging nozzles. This study **aims** to develop and substantiate a comparative validation methodology for assessing the accuracy of simplified analytical isentropic models against high-fidelity computational fluid dynamics (CFD) simulations for two-phase compressible flows involving secondary gas entrainment. The **tasks** to be solved are as follows: implementing a numerical model of the gas-particle flow within a supersonic nozzle using the finite volume method (ANSYS Fluent); performing analytical calculations of particle velocity and temperature using the one-dimensional isentropic model; and conducting a comparative analysis to identify systematic deviations and substantiate the applicability limits of the simplified analytical approach compared to the numerical solution. The **methods** used are: the study of gas dynamics of a two-phase flow was studied by numerical modeling using a modern computing package based on the finite volume method ANSYS Fluent, as well as conventional gas dynamics. The following **results** were obtained: two-phase CFD simulation (carried out in ANSYS Fluent) and a one-dimensional isentropic model were employed to analyze the behavior of nickel particles under varying gas stagnation temperatures (440 °C, 520 °C, 620 °C) and particle diameters (10 μm, 25 μm, 40 μm). The CFD results, which incorporate real gas dynamics, including turbulence, viscous effects, and particle–flow interactions, were compared with analytical results. The CFD results show significantly lower particle velocities (by 50 ± 7%) and higher temperatures (by 22 ± 7%) compared with the isentropic model, primarily due to the inclusion of thermal losses, boundary layer development, and secondary flow effects. The latter arises from the atmospheric entrainment of the carrier gas and powder into the divergent section of the nozzle. These factors disrupt the analytical approach's ideal expansion, reducing the gas and particle velocities while increasing particle temperatures. **Conclusions**. The scientific contribution lies in substantiating that the classic isentropic model reaches its applicability limit for low-pressure cold spray nozzles with downstream injection. The correction coefficients derived from CFD data are proposed to refine analytical models. The practical significance lies in creating a basis for automated design algorithms for supersonic nozzles, enabling the derivation of correction coefficients for analytical equations in the future without the need for repetitive, computationally expensive simulations.*

Keywords: *CFD simulation; gas flow; particle acceleration; ANSYS Fluent; isentropic model.*

1. Introduction

1.1. Motivation

Cold spraying (CS) is a coating technique that imparts specific surface properties to components, such as enhanced wear resistance [1], corrosion resistance [2], and thermal or electrical conductivity [3]. The principal feature of this technology is that coating formation occurs at temperatures below the melting point of the particle material through the high-velocity impact of solid powder particles with the substrate surface [4]. The method has been successfully tested and implemented not only for surface protection but also for repairing damaged components by restoring their functional properties [5].

Ensuring high coating quality requires precise control over the kinetic and thermal energy of powder particles at the moment of impact with the substrate, which serves as the foundation for determining optimal spraying parameters. Although modern Computational Fluid Dynamics (CFD) tools enable high-fidelity predictions of these parameters, they require powerful computing resources, specialized software, and specific expertise. Consequently, isentropic theory-based simplified one-dimensional analytical models are still widely used in engineering practice for rapid nozzle design and parameter optimization.

However, a significant methodological gap exists regarding the validity of these models for complex flow regimes. One of the factors not accounted for in the one-dimensional isentropic gas dynamic model, but which significantly influences the flow dynamics in the nozzle, is the secondary gas entrainment from the atmosphere, along with which the powder is injected. This potentially leads to errors in predicting the velocity and temperature of powder particles in ejector-type nozzles.

ISSN 1814-4225 (print)
ISSN 2663-2012 (online)

Therefore, substantiating the applicability limits of analytical approaches and developing a methodology for validating results and quantifying the error arising from the use of the one-dimensional isentropic model for calculating flow and particle parameters in nozzles designed with an ejector configuration involving secondary flow entrainment remains a pressing issue. Addressing this problem will help prevent nozzle design errors and establish a basis for deriving correction factors for rapid engineering calculations.

1.2. State of the art

The supersonic nozzle is a key component in cold spray systems, significantly influencing the coating quality and overall process efficiency [6].

To ensure high coating performance, powder particles must achieve velocities close to the critical velocity upon impact with the substrate [7]. A well-known one-dimensional isentropic gas dynamic model, as proposed by Dykhuizen [8], may be used to evaluate flow parameters in a supersonic nozzle. The governing equations for determining the gas temperature, pressure, density, and Mach number along the nozzle axis are described in detail in [8, 9]. Once these flow parameters are determined, the temperature and velocity of the entrained powder particles can also be calculated [10].

The model is a valuable tool for approximating the gas and particles' thermal-velocity characteristics. It is particularly useful during the early stages of process design and in defining optimal nozzle channel geometries [11]. The development of the model, particularly by accounting for powder particle size and sphericity in addition to particle impact velocity and temperature, has enabled the prediction of deposition efficiency [12]. However, the model does not account for gas viscosity, turbulence, or boundary layer development along the nozzle walls [13], limiting its applicability in highly precise simulations.

Advancements in computational technologies and modern simulation software have greatly enhanced the study of surface engineering and materials science processes that are difficult or sometimes impossible to analyze experimentally [14, 15]. Numerical modelling of gas dynamics in the CS process using the Reynolds-averaged Navier–Stokes equations offers improved calculation accuracy compared to isentropic models [16]. These equations are based on the conservation laws of mass, momentum, and energy and are well-suited for describing the kinematics of real gas flow while incorporating turbulence and particle-gas interactions [17]. This approach is implemented in applied software tools, such as ANSYS Fluent, which enables the simulation of real gas flows while accounting for compressibility, turbulence, and viscous effects. Furthermore, a distinct advantage of CFD modeling over the one-dimensional isentropic model is the ability to investigate flow mixing within supersonic nozzles [18].

A review of studies on the numerical simulation of gas-dynamic processes in supersonic cold spray nozzles allowed for the generalization of the calculation algorithm for gas and powder particle parameters: discretization of the geometric domain (mesh generation); selection of the mathematical model (e.g., compressible RANS); definition of boundary conditions corresponding to stagnation parameters; and iterative numerical solution until convergence is achieved [19]. This algorithm ensures the reproducibility of results and enables the investigation of flow features that are not accounted for in the isentropic model [20].

The accuracy of such simulations significantly depends on the selected turbulence model. For gas dynamic modelling in CS, commonly used turbulence models include the standard k-ε model, the RNG (Renormalization Group) k-ε model, the Realizable k-ε model, Reynolds Stress Models (RSM), the SST (Shear-Stress Transport) k-ω model, the Spalart–Allmaras model, and others [21].

To describe the interaction between the gas flow and powder particles, either a one-way (uncoupled) or a two-way coupled modelling approach can be used. The one-way approach does not account for powder particle interactions or their influence on the gas flow. The two-way coupled approach considers the effect of the separate phase on the continuous (gas) phase. The one-way Discrete Phase Model (DPM) has been predominantly applied in studies aimed at determining the velocity and temperature of particles during dynamic spraying of cold gas [22].

A review of the literature reveals that most studies aiming to ensure that powder particles of a particular material reach the critical velocity focus either on optimizing nozzle geometry or on defining process parameters through numerical modelling. On the one hand, simplified one-dimensional models provide rapid engineering estimates but neglect the phenomena inherent to the actual flow within a supersonic nozzle, particularly in those designed with an ejector configuration. However, the use of CFD methods, which offer a more accurate assessment of gas and powder parameters within the nozzle, necessitates specialized knowledge, software tools, and computational resources. Currently, systematic studies quantifying the error of analytical approaches when applied to supersonic nozzles with secondary flow entrainment are lacking.

1.3. Objectives and tasks

The transient, nonlinear, and dynamic nature of gas–particle flow near the impact surface makes the

experimental analysis of particle trajectories and behavior is extremely challenging. This underlines the importance of numerical and theoretical investigations.

This study aims to develop and substantiate a comparative validation methodology for assessing the accuracy of simplified analytical isentropic models against high-fidelity CFD simulations for two-phase compressible flows involving secondary gas entrainment.

To achieve the goal, within the framework of this publication, the following tasks must be solved:

1) implement a numerical model of the gas-particle flow within a supersonic nozzle using the finite volume method (ANSYS Fluent);

2) performing analytical calculations of particle velocity and temperature using the one-dimensional isentropic model;

3) conduct a comparative analysis to identify systematic deviations and substantiate the applicability limits of the simplified analytical approach compared to the numerical solution.

The article is organized as follows. Section 2 describes the CFD simulation procedure, describes the governing equations of two-phase flow in a supersonic nozzle, and presents the basic equations of the one-dimensional isentropic model for calculating gas and particle parameters in the flow. Section 3 presents the results of the CFD simulation and analytical model calculation, focusing on the particle velocity and temperature at the nozzle exit. Then, the research findings are compared and explained. Section 4 concludes with a summary of the key findings, including research contributions, and outlines future research directions.

2. Methods of research

2.1. CFD simulation

Low-pressure cold spray nozzle design

Calculations of gas flow parameters and powder particle behavior were performed for both cases at the downstream nozzle of a low-pressure cold spray system. Figure 1 shows a schematic representation of the nozzle, including its geometric dimensions.

The powder is fed perpendicularly to the nozzle axis, entering its divergent section beyond the critical diameter.

Computational model, mesh generation, and boundary conditions setup

The gas flow with powder particles in the supersonic nozzle channel and the submerged region was numerically simulated using ANSYS Fluent 18. The simulation was conducted within the framework of a two-dimensional, axisymmetric problem statement, considering the turbulence of the gas flow and the discrete phase of solid powder particles. Figure 2 shows the computational model. Figure 1 shows the geometric dimensions of the low-pressure cold spray nozzle.

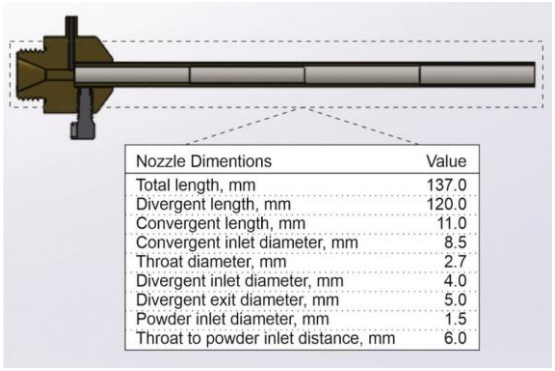

Fig. 1. Schematic views with dimensions of the low-pressure cold spray nozzle

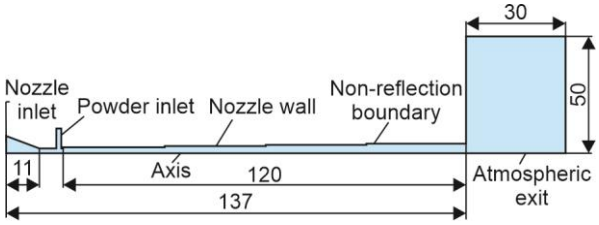

Fig. 2. Computational model for CFD simulation

The total length of the nozzle is 135 mm, and the length of the submerged region beyond the nozzle exit is 30 mm. Powder is injected into the nozzle through a channel located beyond the critical section via an ejector mechanism. The boundary conditions are listed in Table 1.

Table 1

Boundary conditions for CFD simulation.

Location	Pressure P	Velocity V	Temperature T
Nozzle inlet	Defined	$\frac{\partial V}{\partial n}=0$	Defined
Environmental conditions	Normal	$\frac{\partial V}{\partial n}=0$	$\frac{\partial T}{\partial n}=0$
Nozzle wall	$\frac{\partial P}{\partial n}=0$	0	$\frac{\partial T}{\partial n}=0$
Particle inlet channel	Normal	$\frac{\partial V}{\partial n}=0$	Normal

The mesh for the computational domain was generated using the ANSYS WB Meshing Tool. A structured, non-uniform quadrilateral mesh was employed to provide high convergence capabilities. A structured mesh with local thickening in critical areas was generated to ensure an adequate spatial solution of shock waves and boundary layers: in the narrowed part

ISSN 1814-4225 (print)
ISSN 2663-2012 (online)

of the nozzle, near the critical section, and in the expansion zone. The mesh independence was verified by comparing the results for different numbers of nodes, allowing for a compromise between accuracy and computational efficiency.

To improve the resolution of the boundary layer near solid walls, the vertical grid lines were assigned a growth rate of 1.2. A minimum orthogonal quality of 0.7 of mesh elements and a maximum aspect ratio of 30 were set. This mesh density ensured sufficient accuracy in regions with complex flow phenomena. The computational domain consisted of 124,781 elements. To ensure correct modeling of the turbulent boundary layer, the near-wall cell height was defined as 5 μm.

The equations were solved using the SIMPLE scheme with a steady-state formulation with an iterative solution. Convergence control was ensured by controlling the residuals and monitoring variables, including the velocity, temperature, pressure, and particle trajectories. The model was verified based on literature data on particle velocity and flow structure under similar conditions, which were compared with experimental data.

The convergence of the calculations was evaluated by observing the decrease in scaled residuals and the stabilization of monitored variables. Residual targets for the momentum, turbulence, and continuity equations were established at the level of 10^{-5}, and those for the energy equation at 10^{-6} [19]. In addition to evaluating the average velocity and temperature of the gas flow at the nozzle outlet, the mass flow rate balance through the nozzle was monitored. The solution converged once the indicated parameters achieved a steady state with oscillations not exceeding 1% [19].

Governing equations

The motion of compressible gas flow can be described using the Navier–Stokes equations as follows. The following are the governing equations for mass, momentum, energy, and turbulent kinetic energy.

The continuity equation is written as follows

$$\frac{\partial \rho}{\partial t}+\frac{\partial}{\partial x_i}\left(\rho u_i\right)=0, \tag{1}$$

where ρ – gas density;

t – time;

u_i – flow velocity in the i-th direction.

The momentum conservation equation is

$$\frac{\partial}{\partial t}\left(\rho u_i\right)+\frac{\partial}{\partial x_j}\left(\rho u_i u_j\right)= =\frac{\partial}{\partial x_j}\left[-P+\mu_{eff}\left(\frac{\partial u_i}{\partial x_j}+\frac{\partial u_j}{\partial x_i}\right)\right]+S_M, \tag{2}$$

where P – pressure including turbulent normal stress contribution;

S_M – mass or momentum added from the dispersed phase to the gas phase.

The effective viscosity for turbulent flow μ_{eff} is defined as follows:

$$\mu_t=\rho C_\mu \frac{k^2}{\in}, \tag{3}$$

where C_μ = 0,0845 [23].

Turbulent kinetic energy k and dissipation rate $\in$ are obtained using the following transport equations:

$$\frac{\partial}{\partial t}\left(\rho k\right)+\frac{\partial}{\partial x_i}\left(\rho k u_i\right)=\frac{\partial}{\partial x_j}\left[\mu_{eff}\alpha_k\left(\frac{\partial k}{\partial x_j}\right)\right]+ +G_k+G_b-Y_M+S_k-\rho\in, \tag{4}$$

$$\frac{\partial}{\partial t}\left(\rho\in\right)+\frac{\partial}{\partial x_i}\left(\rho\in u_i\right)=\frac{\partial}{\partial x_j}\left[\mu_{eff}\alpha_\in\left(\frac{\partial\in}{\partial x_j}\right)\right]+ +C_{1\in}\frac{\in}{k}\left(G_k+C_{3\in}G_b\right)-C_{2\in}\rho\frac{\in^2}{k}+S_\in-R_\in, \tag{5}$$

where $C_{1\in}$, $C_{2\in}$ and $C_{3\in}$ – turbulence model coefficients [23];

□□ and □□ – inverse effective Prandtl numbers for k and $\in$ respectively;

G_k and G_b – production terms for turbulence due to velocity gradients and buoyancy;

C_k, and $C_\in$, – user-defined source terms.

The additional term $R_\in$, is given as follows

$$R_\in=\frac{C_\mu\rho\eta^3\left(1-\frac{\eta}{\eta_0}\right)}{1+\beta\eta^3}\frac{\in^2}{k}, \tag{6}$$

where $\eta\equiv S_k/\in$;

S – the modulus of the mean rate of the strain tensor;

η_0 = 4,33 and β = 0,012 [23].

The total energy or total enthalpy h_{tot}, adapted for Reynolds-averaged energy equation, is expressed as follows

$$\frac{\partial}{\partial t}\left(\rho h_{tot}\right)-\frac{\partial P}{\partial t}+\frac{\partial}{\partial x_j}\left(\rho u_j h_{tot}\right)=\frac{\partial}{\partial x_j}\left(\lambda\frac{\partial T}{\partial x_j}+\frac{\mu_t}{Pr_t}\frac{\partial h}{\partial x_j}\right)+ +\frac{\partial}{\partial x_j}\left[u_i\left(\tau_{ij}-\rho\overline{u_i u_j}\right)\right]+S_T, \tag{7}$$

where Pr_t – the turbulent Prandtl number;

S_T – the heat exchange source term between the flow and particles;

τ – the stress tensor;

λ – the thermal conductivity.

The enthalpy is related to the total system energy, including the viscous work

$$h_{tot} = C_v T + \frac{1}{2}\left(u_i u_j\right) + k. \quad (8)$$

The additional source terms S_m and S_t in equations (2) and (7) can be neglected because of the low particle concentration in the gas flow. These parameters are excluded from high Stokes numbers and low momentum coupling parameter Π_{mom} [24]. The momentum coupling is expressed as

$$\Pi_{mom} = \frac{z}{\frac{\rho_p d^2 V}{18\mu_g L} + 1}, \quad (9)$$

where subscripts p and g refer to the particle and gas phase parameters, respectively;

d – particle diameter;

L – characteristic length (e.g., nozzle diameter);

Z – powder-to-gas mass flow ratio.

Given that $\rho_g \ll \rho_p$ and a powder feed rate of 0.6 g/s were used in the study, the volume ratio is less than 1%, indicating a negligible influence. Because the concentration of powder fed into the nozzle per unit volume of flow is insignificant, the particle interaction can be neglected.

The solid phase was simulated as individual particles using a Lagrangian approach [24]. A pressure-based solver was used. Gradient calculations were performed using the Green-Gauss node-based method. Second-order pressure discretization was employed, and the QUICK scheme was utilized to solve the density and momentum equations.

Turbulence model

In supersonic flow, due to the high flow velocities, inertial forces are expected to dominate over viscous dissipation, leading to high Reynolds numbers. Consequently, the flow is considered turbulent. In simulations of gas flow for cold gas dynamic spraying, Reynolds-averaged Navier–Stokes (RANS) equations are used, and various turbulence models are applied to close the system of equations.

Each of these models contains a set of valid empirical constants under specific flow conditions. A given turbulence model generally yields accurate results only for a particular class of flows. In this study, the RNG k-ε turbulence model was selected because it provides sufficiently accurate results for gas flow calculations.

The employed model yields time-averaged characteristics, which represent a certain limitation. Compared with other models (e.g., LES, DNS), RANS provides less detailed information regarding instantaneous flow turbulence within the nozzle. However, it is sufficient to determine the mean velocity fields necessary to estimate the acceleration of powder particles in the nozzle [6, 10].

Although turbulence is inherently a three-dimensional phenomenon, a two-dimensional axisymmetric formulation was applied to reduce computational time. This choice is justified by the nozzle's geometric symmetry and provides sufficient accuracy for determining the velocity of powder particles in the flow [10].

Discrete phase (powder particles)

Nickel powder particles were introduced into the gas flow through a powder injection channel oriented perpendicular to the nozzle axis (see figure 1). The forces and heat transfer from the flow to the particles were calculated using Newton's second law and the energy balance equation. The drag coefficient was calculated using the equations reported by Henderson [25]. A two-phase flow simulation was conducted using a combined Lagrangian approach.

The drag force balance was used to calculate the velocity and trajectory of the discrete phase, i.e., nickel particles in the two-phase flow. Other forces, such as gravity, lift, and electrostatic forces, were not included in the calculation because they have an insignificant impact on particle momentum during CS (see para. 2.2).

To determine the drag coefficient C_D as a function of the particle Mach number, the following equations were used [25]. The correlations presented in [25], which cover a wide range of Mach and Reynolds numbers, provided accurate results based on two-phase flow experimental studies [10, 26].

The energy balance equation from the first law of thermodynamics was used to model transient heat transfer processes [10, 27].

The average convective heat transfer coefficient was calculated using the Nusselt number

$$\overline{Nu} = 2 + 0,44\,Re^{0,5}\,Pr^{0,33}\exp\left(0,1 + 0,872M_p\right). \quad (10)$$

Equation (10) is applied when the Mach number of the particle exceeds 0.24. The general Ranz–Marshall model is used in all other cases [28].

2.2. Analytical models

One-dimensional isentropic model for gas flow parameters in a nozzle

A gas flow in which significant changes in density (dρ) occur due to pressure (dP) and temperature (dT) changes is referred to as a compressible flow. The rate of

ISSN 1814-4225 (print)
ISSN 2663-2012 (online)

change in density with respect to pressure can be related to the speed of sound. Sound is defined as an infinitesimally small pressure wave that causes changes in pressure, density, and velocity as it continuously propagates through a medium. Its speed is the distance the pressure wave travels per unit time in a given medium. Assuming that the flow is composed of an ideal gas, described by the ideal gas law, we have

$$P = \rho RT, \tag{11}$$

the speed of sound c_g of an ideal gas can be obtained using the following formula

$$c_g = \sqrt{\gamma RT}, \tag{12}$$

where R – the specific gas constant;

γ – the adiabatic index (ratio of specific heats).

Equation (12) shows that the speed of sound in an ideal gas depends solely on the gas temperature T and the specific heat ratio γ. Thus, the higher the temperature and specific heat, the higher the achievable gas velocity at the nozzle exit.

The effect of sound speed on compressibility and pressure pulses can be evaluated using the Mach number as follows:

$$M = \frac{V}{c}. \tag{13}$$

Table 2 presents the initial data for the calculation.

Table 2

Initial parameters for the calculation

Parameter	Value
Powder particle:	
material	Nickel
density ρ_p, kg/m^3	8874
diameter d_p, um	10; 25; 40
specific heat C_p, J/kg·K	446
initial temperature T_{p0}, K	293
Working gas (air):	
specific gas constant R, J/kg·K	287.05
adiabatic index γ	1.4
stagnation temperature T_0, °C	440; 520; 620
stagnation pressure P_0, MPa	0.9
Powder transporting gas (air):	
specific gas constant R, J/kg·K	287.05
adiabatic index γ	1.4
stagnation temperature T, °C	293
stagnation pressure P, MPa	0.1

In a simplified analysis, the following assumptions are made:

1) The gas flow is isentropic: both heat exchange and frictional effects are negligible. Therefore, the flow can also be considered reversible and hence isentropic.

2) The gas flow is one-dimensional: gas properties are uniform in the direction perpendicular to the flow.

3) The gas behaves as an ideal gas.

4) The specific heats at constant pressure ($dh = C_p dT$) and constant volume ($du = C_v dT$) are assumed to be constant; i.e., the gas is calorically ideal.

If the flow within the nozzle is considered a control volume with no external energy or work input, and is characterized by stagnation pressure and temperature, then, assuming negligible heat and friction losses, the first law of thermodynamics can be written in terms of the control volume's stagnation enthalpy

$$h_0 = h + \frac{V^2}{2} = \text{const}, \tag{14}$$

where h_0 – the enthalpy of the flow at zero velocity;

V – the flow velocity.

Assuming a constant specific heat at a constant pressure and using the ideal gas law, the following relationship is obtained:

$$C_p = \frac{\gamma R}{(\gamma - 1)}. \tag{15}$$

If the stagnation temperature T_0 and stagnation pressure P_0 are set as the initial conditions, the gas density can be derived from the ideal gas equation

$$\rho_0 = \frac{P_0}{RT_0}. \tag{16}$$

The gas temperature, pressure, and density at any point within the nozzle can be determined using the following isentropic relations:

$$\frac{T_0}{T} = 1 + \frac{\gamma - 1}{2} M^2, \tag{17}$$

$$\frac{P_0}{P} = \left(1 + \frac{\gamma - 1}{2} M^2\right)^{\frac{\gamma}{\gamma - 1}}, \tag{18}$$

$$\frac{\rho_0}{\rho} = \left(1 + \frac{\gamma - 1}{2} M^2\right)^{\frac{\gamma}{\gamma - 1}}. \tag{19}$$

When the sonic condition is reached at the throat, the stagnation pressure P_0 and the gas properties at the critical section (temperature T*, velocity V*, and density ρ*) can be calculated as follows:

$$T^* = \frac{T_0}{1 + (\gamma - 1)/2}, \text{ at } M^* = 1, \tag{20}$$

$$V^* = \sqrt{\gamma RT^*}, \tag{21}$$

$$\rho^* = \frac{m^*}{V^* A^*}, \tag{22}$$

where A^* is cross-sectional area of the nozzle throat.

Additionally, the pressure in the critical section can be calculated using the ideal gas law

$$P^* = \rho^* R T^*. \quad (23)$$

The ratio of the cross-sectional areas of the nozzle to the Mach number can be expressed as follows:

$$\frac{A}{A^*} = \frac{1}{M}\left[\frac{1}{(\gamma-1)}\left(1+\frac{(\gamma+1)}{2}M^2\right)\right]^{\frac{(\gamma+1)}{2(\gamma-1)}}, \quad (24)$$

from which the Mach number at the nozzle exit can be obtained. In commercial systems, the critical cross-sectional area A* of CS nozzles typically ranges from 1.0 to 3.0 mm^2, depending on the system's maximum gas flow rate and the power of the gas heater.

The calculations presented in this section were based on isentropic assumptions. In reality, however, flow behavior in the nozzle is also influenced by friction, heat losses, and gas viscosity [29]. These effects reduce the available enthalpy that can be converted into kinetic energy, lowering the velocity of the exit gas. The presence of a boundary layer on the nozzle walls may reduce the gas velocity to as low as 67% of the theoretical isentropic value [30]. Using longer nozzles in CS helps to minimize disturbances caused by the boundary layer and improves flow quality at the nozzle exit [30].

Calculation of powder particle parameters in the gas flow

To determine the velocity of a powder particle in the gas flow during cold gas dynamic spraying, the following expression can be used [31]

$$m_p \frac{dV_p}{dt} = \frac{1}{2} C_D \rho_g A_p \left(V_g - V_p\right)^2 + F_b, \quad (25)$$

where m_p – particle mass;
V_p – particle velocity;
C_D – drag coefficient;
ρ_g – particle density;
V_g – gas velocity;
A_p – particle cross-sectional area
F_b – body forces.

Body forces include gravitational [31], lift [32], electrostatic [31], and adverse pressure gradients due to shock waves [26].

The Reynolds number and the Mach number of a particle can be calculated using the following relationships [31]

$$Re_p = \frac{\rho_g \left|V_g - V_p\right|}{\mu_g} \quad (26)$$

and

$$M_p = \frac{\left|V_g - V_p\right|}{c} = \frac{|\Delta V|}{\sqrt{\gamma R_g T_g}}, \quad (27)$$

where subscripts g and p refer to the gas and the particle, respectively, and denotes the gas's dynamic viscosity.

$$\mu = \frac{C_1 T_f^{3/2}}{T_f + C_2}, \quad (28)$$

where C_1 and C_2 are equal to 1,663*10^{-5} kg/m·s·K$^{1/2}$.

Using the equation for the speed of sound in an ideal gas (equation (12)), the Mach number (equation (13)), and the ideal gas law, the particle acceleration can be expressed as follows:

$$a_p = \frac{P_0}{2RT_0}\left(1+\frac{\gamma-1}{2}M^2\right)^{\frac{-1}{\gamma-1}} \times$$
$$\times\left(M\sqrt{\gamma R T_0\left(1+\frac{\gamma-1}{2}M^2\right)^{-1}} - V_p\right)^2 C_D \frac{A_p}{2Vol_p\rho_p}. \quad (29)$$

Accurate determination of the drag coefficient over a wide range of flow regimes is necessary for a more precise particle velocity calculation in the CS process.

To determine the temperature of a particle in the gas flow during CS, the average convective heat transfer coefficient, which accounts for the flow characteristics around the particle surface, must be evaluated. The overall heat exchange at the particle surface can be expressed as follows [31]:

$$q = \bar{h} A_s \left(T_w - T_p\right) \quad (30)$$

and

$$\bar{h} = \frac{1}{A_s}\int_{A_s} h dA_s, \quad (31)$$

where A_s – the surface area of the particle;
T_w – the gas temperature at the boundary layer (wall).

The non-dimensional temperature gradient, represented by the Nusselt number, can be calculated as follows [31]

$$\overline{Nu} = \frac{\bar{h} d_p}{k_g}, \ \overline{Nu} = f\left(Re_p, M_p, Pr\right), \quad (32)$$

where k_g – the thermal conductivity of the gas;
d_p – the particle diameter.

The convective heat transfer coefficient can be calculated once the Nusselt number is determined. For simplification, the Ranz-Marshall correlation is commonly used in CS simulations

ISSN 1814-4225 (print)
ISSN 2663-2012 (online)

$$Nu = 2 + 0.6\,Re^{0.5}\,Pr^{0.33}, \quad (33)$$

where Pr is the Prandtl number.

However, the Ranz-Marshall correlation was originally developed for low Reynolds numbers (0–200) and Mach numbers [31]; therefore, it does not account for compressibility, rarefaction, and Mach number effects relevant to supersonic two-phase flows. Other models have been proposed in the literature that incorporate Knudsen number Kn_p, Reynolds number Re_p, and Mach number M_p into the heating process. Nonetheless, the accuracy of these measurements remains unverified due to the difficulty in experimentally measuring particle temperature during CS.

Assuming a uniform particle temperature, the first law of thermodynamics yields the following:

$$m_p \frac{dT_E}{dt} = A_{s.p}\bar{h}\left(T_r - T_p\right), \quad (34)$$

where m_p – particle mass;

C_p – specific heat of the particle;

$A_{s.p}$ – particle surface area;

T_r – recovery temperature.

The recovery temperature is defined as the temperature in the boundary layer surrounding the particle during flight

$$T_r = T_g\left(1 + r\frac{\gamma - 1}{2}M_p^2\right), \quad (35)$$

where r is the recovery factor, which is typically close to 1.0 for gases [31].

The recovery factor for Reynolds numbers around 2000 can be estimated as follows:

$$r = \sqrt{Pr} = \sqrt{\left(\frac{\mu_{g,f}C_{p(g,f)}}{k_{g,f}}\right)}, \quad (36)$$

where Pr – the Prandtl number;

k_g – the thermal conductivity of the gas, which is a function of temperature, and can be calculated using the following relation [5]:

$$k = \frac{9\gamma - 5}{4}\frac{C_v}{\pi d^2}\sqrt{\frac{Mk_BT_r}{N\pi}}, \quad (37)$$

where N – Avogadro's number, N = 6,022*10^{23} molecules/mol,

k_B – Boltzmann constant, k_B = 1,381*10^{-23} J/K;

d – the molecular diameter of a gas;

M – the molecular mass.

3. Results and Discussion

3.1. CFD simulation results

The results of CFD simulation of the gas flow in and beyond the nozzle are shown below. As examples, Figure 3 shows the contours of velocity (Figure 3a) and temperature (Figure 3b) at 520 °C and 0.9 MPa.

The contour plots illustrate the effect of entrained flow through the powder injection channel on the flow acceleration front and temperature distribution. The stepped shape of the diverging section of the nozzle initiates a series of shock waves that slow down the gas flow.

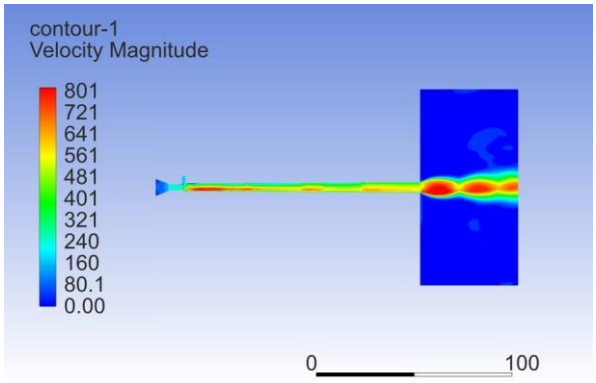

a

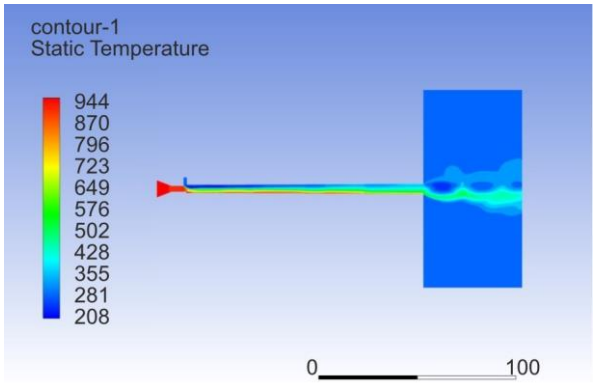

b

Fig. 3. Gas parameter distributions from CFD results at 520 °C and 0.9 MPa: a – velocity – and b – temperature

Figure 4 presents the trajectories, velocity, and temperature changes of the injected nickel powder particles (10 μm) inside and beyond the nozzle at 620 °C and 0.9 MPa.

Most particles do not strictly follow the axis of the nozzle. The peripheral gas flows slower than the central flow, resulting in lower impact velocities for off-axis particles.

Figures 5 and 6 show the graphs of temperature and velocity changes for the nickel particles (10 μm, 25 μm, and 40 μm) along and beyond the nozzle axis for 440 °C, 520 °C, and 620 °C at 0.9 MPa.

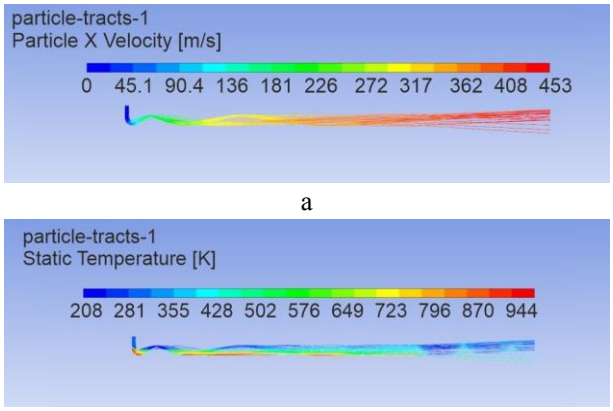

Fig. 4. Nickel particle (10 μm) trajectory at 620 °C and 0.9 MPa: a – velocity and b – temperature

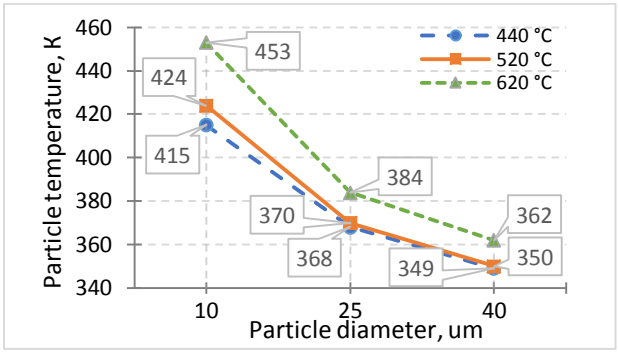

Fig. 5. Temperature of the nickel particles at the nozzle exit (CFD simulation)

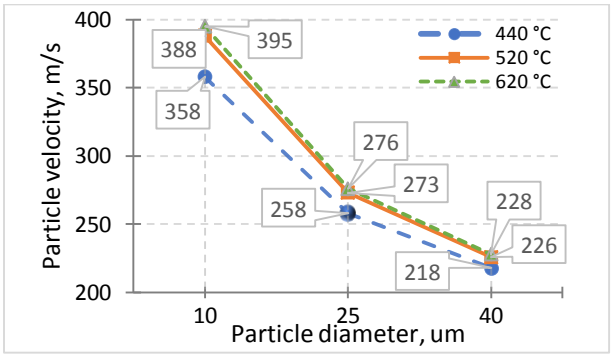

Fig. 6. The velocity of the nickel particle at the nozzle exit (CFD simulation)

As particles enter the nozzle, they are heated and accelerated. With stagnation temperature increasing from 440 °C to 620 °C at constant pressure, the exit velocities of nickel particles (10 μm, 25 μm, and 40 μm) rise from 358 m/s, 258 m/s, and 218 m/s to 395 m/s, 276 m/s, and 228 m/s. The particle temperatures increased from 415 K, 368 K, and 349 K to 453 K, 384 K, and 362 K, respectively. This increase in velocity is due to the increasing velocity of the gas. CFD results also show that as the particle diameter increases from 10 μm to 40 μm, both the velocity and temperature at the nozzle exit decrease due to the increased mass and cross-sectional area.

From equation (19), it is evident that the gas density decreases as the Mach number increases. A decrease in density results in a lower drag force acting on the particles moving within the flow, which in turn reduces their velocity. Therefore, the expansion of gas to very high Mach numbers inside a converging-diverging nozzle does not necessarily guarantee high particle velocities. Therefore, the CS process is typically operated in a supersonic flow regime with Mach numbers in the range of 2.0 to 3.0, rather than in the hypersonic regime.

High-pressure systems are used in practice to increase the gas density and improve particle acceleration, where the gas stagnation pressure may reach up to 5 MPa. However, equation (29) also shows that the particle momentum in the gas flow depends on the particle material and size [33].

3.2. Results of one-dimensional isentropic model calculation

The following are the results of calculations for the velocity and temperature of gas and nickel powder particles in the channel of the converging-diverging supersonic LPCS nozzle (see Figure 1), obtained using a one-dimensional isentropic model.

Figures 7 and 8 show the calculated temperatures and velocities of the gas and nickel particles in the nozzle, respectively.

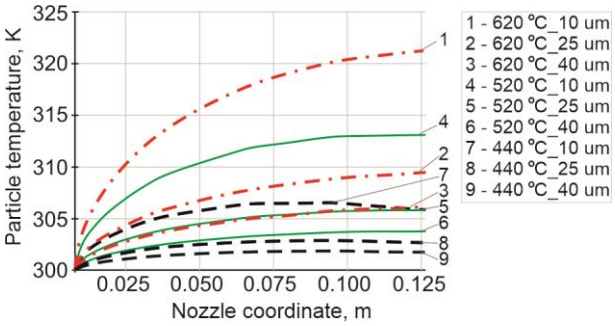

Fig. 7. Temperature of gas and nickel particles in the nozzle (isentropic model)

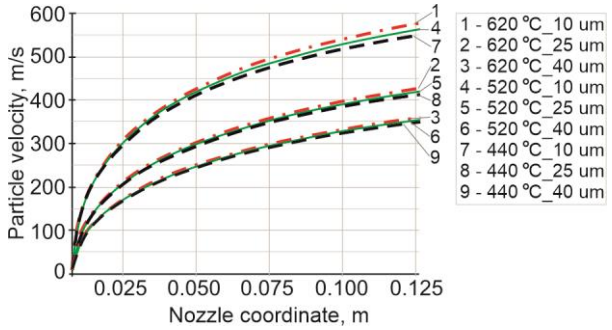

Fig. 8. Gas and nickel particle velocity in the nozzle (isentropic model)

ISSN 1814-4225 (print)
ISSN 2663-2012 (online)

The graphs illustrate the conversion of thermal energy into kinetic energy in the nozzle's converging and diverging sections. As the gas temperature in the converging section decreases, its velocity increases. After passing the critical diameter, the gas temperature continues to drop while the velocity increases sharply.

Powder is injected into the diverging section of the nozzle (see Figure 1). As the gas velocity in the diverging section increases, the particle velocity also increases. Figure 6 shows that increasing the particle diameter results in lower velocities. For nickel particles with diameters of 10 μm, 25 μm, and 40 μm, the exit velocities are 551 m/s, 413 m/s, and 350 m/s, respectively, at 0.9 MPa and 440 °C.

When the temperature is increased to 620 °C with a constant pressure of 0.9 MPa, these values increase to 558 m/s, 428 m/s, and 360 m/s.

The particle exit temperature also depends on the diameter and increases with size. At 440 °C particle temperatures are 306 K, 303 K, and 302 K for diameters of 10 μm, 25 μm, and 40 μm, respectively. At 620 °C and 0.9 MPa, these values increase to 321 K, 309 K, and 306 K.

3.3. Comparison of results obtained from the CFD simulation and the isentropic model

The gas parameters are a function of the nozzle geometry, stagnation temperature, and stagnation pressure. The flow is decelerated and then accelerated due to variations in the nozzle cross-sectional area, which influence the local Mach number. The velocity of the powder particles achieved within the nozzle during the deposition process is limited by the gas velocity. At constant stagnation pressure, an increase in the stagnation temperature at the nozzle inlet leads to an increase in the gas velocity along the nozzle channel. Equation (12) describes the dependence of the gas velocity on its temperature. Consequently, an increase in the velocity of powder particles introduced into the divergent section of the nozzle is observed, regardless of their diameter.

Considering equation (25), the particle velocity is not only limited by the gas velocity but also increases monotonically with the time the particle spends in the flow. This justifies the use of long nozzles in cold spray processes because the longer the particle travels within the flow, the higher its resulting velocity. It is also important to note that the optimal conditions for particle acceleration are determined by the condition of the maximum drag force, meaning that particle acceleration depends on the gas density, which increases as the density increases.

Regarding particle diameter, an optimal size exists, depending on the gas flow parameters and nozzle geometry, at which particle velocity reaches its maximum. Given that powders are characterized by a certain size distribution with a known mean diameter and standard deviation, it is crucial that the average particle size must correspond to this optimal diameter. This allows for the achievement of maximum deposition efficiency.

Table 3 summarizes the calculation results for the velocity and temperature of nickel powder particles obtained using the isentropic model and numerical modeling.

Table 3

Summary of nickel particle velocity and temperature

Particle diameter, um	CFD simulation			Isentropic model		
	Gas stagnation temperature, °C					
	440	520	620	440	520	620
Particle velocity, m/s						
10	353	388	395	551	564	578
25	258	273	276	413	420	428
40	218	226	228	350	355	360
Particle temperature, K						
10	415	424	453	306	313	321
25	368	370	384	303	306	309
40	349	350	362	302	304	306

Comparing the results obtained from the analytical model with those from CFD simulations, the one-dimensional isentropic model significantly overestimated particle velocity (by approximately $50 \pm 7\%$) and underestimated particle temperature (by approximately $22 \pm 7\%$) relative to the results from CFD simulations in ANSYS Fluent. These discrepancies can be attributed to several simplifying assumptions used in the analytical model, including one-dimensional and isentropic flow, the absence of particle–flow interaction, and ideal expansion (i.e., full conversion of thermal energy into kinetic energy). The one-dimensionality assumption implies purely axial flow without transverse velocity components along the nozzle axis. Isentropicity assumes that the model neglects heat losses, viscosity, thermal conductivity, friction, turbulence, and vortical structures, all of which significantly affect the actual flow behaviour.

Unlike the isentropic model, the CFD model accounts for real physical phenomena, such as heat transfer, gas viscosity, particle inertia, and the three-dimensional nature of the flow, making its results more representative of actual conditions. This explains the significant differences in the predicted particle velocities and temperatures. The gas viscosity and the boundary layer along the nozzle walls reduce the flow velocity. Turbulence introduces additional energy losses, heat transfer occurs between the flow and the nozzle walls, and local flow disturbances can be generated by the nozzle geometry.

Moreover, CFD simulation enables the analysis of the two-phase flow, including the thermal interaction between the gas and particles. In contrast, the isentropic model often assumes that particles follow the gas flow perfectly (zero-slip assumption), meaning they instantaneously accelerate to match the gas velocity. CFD modeling, however, accounts for particle inertia; particles only adjust their velocity if they are sufficiently light. Similarly, heat exchange between particles and gas is calculated in detail in CFD simulations, whereas it is often approximated or neglected in simplified models.

Notably, the flow parameters at the nozzle exit do not necessarily match the ideal conditions at the theoretical exit plane. The isentropic model assumes perfect expansion to the calculated exit pressure. In reality, overexpansion or underexpansion may occur, especially if the exit pressure is not perfectly matched to the ambient pressure.

The presence of a secondary flow, which enters the main flow from the atmosphere along with powder particles in the divergent section of the nozzle, downstream of the throat, is a particularly important factor explaining the discrepancies between CFD results and the analytical model. This effect is not considered in the isentropic model, which defines the velocity and temperature of particles based solely on their coordinates along the nozzle axis. In the real cold spray process, powder is introduced without heating and transported from an open-type powder feeder by atmospheric air via ejector suction. Therefore, the carrier gas's temperature and pressure correspond to ambient (standard) conditions.

The properties of the primary flow are affected by the presence of such a secondary flow in low-pressure supersonic cold spray nozzles, operating according to the ejector scheme (with powder introduced into the divergent section). This ambient-temperature, ambient-pressure flow disrupts the main flow's isentropic nature, reduces the gas temperature and velocity due to cooling and turbulent mixing, and introduces additional disturbances and energy losses. As a result, the flow parameters and particle dynamics near the nozzle exit significantly differ from those predicted by the one-dimensional model, which explains the lower velocities and higher temperatures observed in CFD simulations.

3.4. CFD model validation

The model employed in this study was validated by reproducing the computational conditions previously presented by other authors. A comprehensive validation of the CFD model and a thorough analysis of the gas-particle flow simulation results in a cold spray nozzle, verified experimentally, are presented in [10].

The computational conditions from the aforementioned publications were reproduced in the current study, including nozzle geometry, boundary conditions, and the physical properties of the gas and particles.

Figure 9 presents a comparison between the replicated simulation results obtained by the current authors (green dots), the original results from [10] (red dots), and their experimental data [10]. In Figure 9, PSV denotes Particle Streak Velocimetry, PTV stands for Particle Tracking Velocimetry, and CSM refers to the Cold Spray Meter [34].

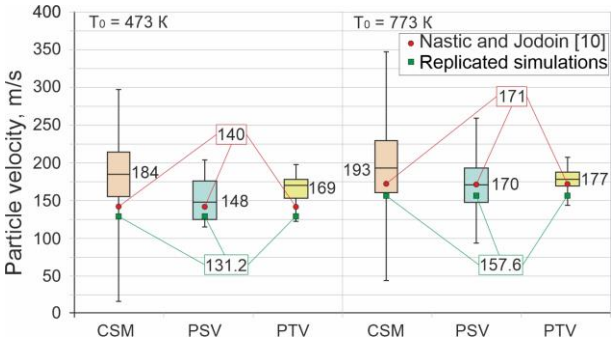

Fig. 9. Results of the replicated simulations and comparison with the original data

The results presented in Figure 9 confirm the validity of the numerical model employed and the selection of physical and computational parameters. Based on this, the applied CFD model adequately describes the gas flow and particle behavior, and is suitable for calculations within the scope of the problem under consideration.

4. Conclusions

This study was conducted to develop and substantiate a methodology for validating simplified analytical models of gas-dynamic processes in supersonic converging-diverging spray nozzles using CFD simulation. This study focused on a specific case: an ejector nozzle for low-pressure cold gas dynamic spraying with secondary flow entrainment into the divergent section of the nozzle, for which traditional one-dimensional assumptions are often violated.

It has been scientifically substantiated that the classical isentropic model reaches the limit of its applicability for nozzles with secondary gas entrainment. Correction coefficients must be introduced to refine it, which can be derived using CFD modeling. The proposed methodology enables a quantitative assessment of the error in calculating powder particle velocity and temperature, which results from the simplifications adopted in the analytical model. The isentropic model overestimates particle velocities by 50 ± 7% and underestimates particle temperatures by 22 ± 7% compared to the CFD results, which account for

ISSN 1814-4225 (print)
ISSN 2663-2012 (online)

turbulence, viscous effects, boundary layers, gas–particle interactions, and the carrier gas flow.

Unlike high-pressure cold spray nozzles with powder injection into the subsonic section – where the analytical model can be applied for preliminary estimation of gas and particle parameters –the design of low-pressure ejector nozzles requires the use of 2D/3D CFD models to account for shock wave structures and secondary flow interactions.

The proposed methodology provides a foundation for the development of automated design algorithms for supersonic spray nozzles, enabling the derivation of correction coefficients for analytical equations without the need for repetitive, computationally expensive simulations in the future.

Contributions of authors: conceptualization, methodology, formulation of tasks – **Oleksandr Shorinov;** model run – **Nina Savchenko**; CFD simulation – **Sergii Polyviany;** analysis of results – **Oleksandr Shorinov, Sergii Polyviany;** original draft preparation – **Oleksandr Shorinov**; writing – review and editing **– Nina Savchenko, Roman Ipatov.**

Conflict of Interest

The authors declare that they have no conflict of interest in relation to this research, whether financial, personal, authorship, or otherwise, that could affect the research and its results presented in this paper.

Financing

This study was conducted without financial support.

Data Availability

The work has associated data in the data repository.

Use of Artificial Intelligence

The authors confirm that they did not use artificial intelligence methods while creating the presented work.

All the authors have read and agreed to the published version of this manuscript.

References

1. Jafari, R., Cizek, J., Lukac, F., Cvrcek, L., Buril, M., Walter, J., Honkanen, M., Vippola, M., & Koivuluoto, H. A Comparative Study on Wear Resistance of Cold-Sprayed Aluminum/Quasicrystal Composite Coatings. *Journal of Thermal Spray Technology*, 2024, vol. 33, pp. 705–718. DOI: 10.1007/s11666-024-01758-8.

2. Zhang, M., Zhou, S., Huang, R., Xu, F., Wang, J., Dai, S., Zhang, Y., & Zhu, L. Cold sprayed Cu-coated AlN reinforced copper matrix composite coatings with improved tribological and anticorrosion properties. *Surface and Coatings Technology*, 2025, vol. 496, article no. 131666. DOI: 10.1016/j.surfcoat.2024.131666.

3. Liu, Q., Gong, C., Zhou, C., Liang, T., Hao, Z., Wang, Z., & Tian, X. Comparative analysis of mechanical and electrical properties of graphene/copper composite coating on PEEK via cold spray with varied nozzle speed. *Journal of Thermal Spray Technology*, 2024, vol. 33, pp. 2209–2226. DOI: 10.1007/s11666-024-01853-w.

4. Assadi, H., Kreye, H., Gärtner, F., & Klassen, T. Cold spraying – a materials perspective. *Acta Materialia*, 2016, vol. 116, pp. 382–407. DOI: 10.1016/ j.actamat.2016.06.034.

5. Dayı, S. C., & Kılıçay, K. Repairing Al7075 surface using cold spray technology with different metal/ceramic powders. *Surface and Coatings Technology*, 2024, vol. 489, article no. 131124. DOI: 10.1016/j.surfcoat.2024.131124.

6. Falco, R., & Bagherifard, S. Cold spray additive manufacturing: a review of shape control challenges and solutions. *Journal of Thermal Spray Technology*, 2025, vol. 34, pp. 1023–1041. DOI: 10.1007/s11666-025-01970-0

7. Schmidt, T., Gärtner, F., Assadi, H., & Kreye, H. Development of a generalized parameter window for cold spray deposition. *Acta Materialia*, 2006, vol. 54, no. 3, pp. 729–742. DOI: 10.1016/j.actamat.2005.10.005.

8. Dykhuizen, R. C., & Smith, M. F. Gas dynamic principles of cold spray. *Journal of Thermal Spray Technology*, 1998, vol. 7, no. 2, pp. 205–212. DOI: 10.1361/105996398770350945.

9. Martinez-Flores, M., Cervantes-Cabello, J. J., & Barba-Pingarron, A. Low-pressure cold spray deposition window derived from a one-dimensional analytical model. *Coatings*, 2023, vol. 13, no. 6, article no. 1015. DOI: 10.3390/coatings13061015.

10. Nastic, A., & Jodoin, B. Evaluation of heat transfer transport coefficient for cold spray through computational fluid dynamics and particle in-flight temperature measurement using a high-speed IR camera. *Journal of Thermal Spray Technology*, 2018, vol. 27, no. 8, pp. 1491–1517. DOI: 10.1007/s11666-018-0787-y.

11. Shorinov, O., Volkov, A., Neveshkin, Y., Danko, K., & Kalinichenko, N. Theoretical study of powder particle parameters in a modified cold spray nozzle. *Advances in Design, Simulation and Manufacturing VI*, 2023, pp. 168–176. DOI: 10.1007/978-3-031-32774-2_17.

12. Ozdemir, O. C., & Muftu, S. Novel method of predicting deposition efficiency in cold spray by incorporating sphericity into 1D numerical models. *Thermal Spray 2022: Proceedings from the International Thermal Spray Conference*, Vienna, Austria, May 4–6, 2022, pp. 389–394. DOI: 10.31399/asm.cp. itsc2022p0389.

13. Alonso, L., Garrido-Maneiro, M. A. & Poza, P. A study of the parameters affecting the particle velocity in cold-spray: Theoretical results and comparison with experimental data. *Additive Manufacturing*, 2023, vol. 67, article no. 103479. DOI: 10.1016/j.addma. 2023.103479.

14. Tryfonov, O., Shypul, O., Garin, V., Myntiuk, V. & Tkachenko, D. A numerical simulation study of hydrogen-air mixture combustion in a closed chamber at low initial pressure. *Radioelectronic and Computer Systems*, 2024, no. 4, pp. 259–269. DOI: 10.32620/reks.2024.4.21

15. Shorinov, O. Finite element analysis of thermal stress in Cu_2 O coating synthesized on Cu substrate. *Archives of Materials Science and Engineering*, 2022, vol. 115, no. 2, pp. 58–65. DOI: 10.5604/ 01.3001.0016.0753.

16. Gutiérrez de Frutos, J., List, A., Nielsen, S., Gärtner, F., & Klassen, T. Nozzle geometry evaluation for cold spray applications by using 3D-CFD Calculations. *J Therm Spray Tech*, 2025, vol. 34, pp, 570–586. DOI: 10.1007/s11666-025-01945-1.

17. Gabor, T., Akin, S., & Byung-Guk Jun, M. Numerical studies on cold spray gas dynamics and powder flow in circular and rectangular nozzles. *Journal of Manufacturing Processes*, 2024, vol. 114, pp. 232–246. DOI: 10.1016/j.jmapro.2024.02.005.

18. Sharma, A. K., Vashishtha, A., Callaghan, D., Bakshi, S. R., Kamaraj, M., & Raghavendra, R. CFD investigation of a co-flow nozzle for cold spray additive manufacturing applications. *Journal of Thermal Spray Technology*, 2024, vol. 33, pp. 1251–1269. DOI: 10.1007/s11666-024-01764-w.

19. *Ansys Fluent Theory Guide, Release 2025 R2*. Canonsburg, PA, USA, Ansys, Inc., 2025. Available at: ansyshelp.ansys.com (last accessed 12.05.2025).

20. Badali, P., Rahmanpour, M. & Hashemi, M.Y. Numerical study of nozzle geometry effect on cold spray performance. *Computational Particle Mechanics*, 2025, vol. 12, pp. 3487–3497. DOI: 10.1007/s40571-025-01035-7.

21. Shorinov, O., Volkov, A., Dolmatov, A., Balushok, K.; Tonkonogyi, V., Ivanov, V., Trojanowska, J., Oborskyi, G., & Pavlenko, I. *Numerical Simulation of a Modified Nozzle for Cold Spraying*. Advanced Manufacturing Processes V. Cham: Springer, 2023, pp. 571–579. DOI: 10.1007/978-3-031-42778-7_53.

22. Yin, S., Meyer, M., Li, W., Liao, H., & Lupoi, R. Gas Flow, Particle Acceleration, and Heat Transfer in Cold Spray: A review. *Journal of Thermal Spray Technology*, 2016, vol. 25, no. 5, pp. 874–896. DOI: 10.1007/s11666-016-0406-8.

23. Nastic, A., Jodoin, B., Poirier, D., & Legoux, J. G. Particle temperature effect in cold spray: A study of soft particle deposition on hard substrate. *Surface and Coatings Technology*, 2021, vol. 406, article no. 126735. DOI: 10.1016/j.surfcoat.2020.126735.

24. Tabbara, H., Gu, S., McCartney, D. G., Price, T. S., & Shipway, P. H. Study on Process Optimization of Cold Gas Spraying. *Journal of Thermal Spray Technology*, 2010, vol. 20, no. 3, pp. 608–620. DOI: 10.1007/s11666-010-9564-2.

25. Henderson, C. B. Drag Coefficients of Spheres in Continuum and Rarefied Flows. *AIAA Journal*, 1976, vol. 14, no. 6, pp. 707–708. DOI: 10.2514/3.61409.

26. Champagne, V. K., Helfritch, D. J., Dinavahi, S. P. G., & Leyman, P. F. Theoretical and Experimental Particle Velocity in Cold Spray. *Journal of Thermal Spray Technology*, 2010, vol. 20, no. 3, pp. 425–431. DOI: 10.1007/s11666-010-9530-z.

27. Birt, A. M., Champagne, V. K., Sisson, R. D. & Apelian, D. Microstructural analysis of Ti–6Al–4V powder for cold gas dynamic spray applications. *Advanced Powder Technology*, 2015, vol. 26, no. 5, pp. 1335–1347. DOI: 10.1016/j.apt.2015.07.008.

28. Stoltenhoff, T., Kreye, H., & Richter, H. J. An Analysis of the Cold Spray Process and Its Coatings. *Journal of Thermal Spray Technology*, 2002, vol. 11, no. 4, pp. 542–550. DOI: 10.1361/105996302770348682.

29. Carling, J. C., & Hunt, B. L. The near wall jet of a normally impinging, uniform, axisymmetric, supersonic jet. *Journal of Fluid Mechanics*, 1974, vol. 66, no. 1, pp. 159–176. DOI: 10.1017/ s0022112074000127.

30. Alkhimov, A. P., Kosarev, V. F., & Klinkov, S. V. The Features of Cold Spray Nozzle Design. *Journal of Thermal Spray Technology*, 2001, vol. 10, no. 2, pp. 375–381. DOI: 10.1361/105996301770349466.

31. Nastic, A., MacDonald, D., & Jodoin, B. The influence of feedstock powder. In: *Materials Forming, Machining and Tribology*. Cham: Springer International Publishing, 2020, pp. 33–85. DOI: 10.1007/978-3-030-42756-6_3.

32. Jen, T.-C., Li, L., Cui, W., Chen, Q., & Zhang, X. Numerical investigations on cold gas dynamic spray process with nano- and microsize particles. *International Journal of Heat and Mass Transfer*, 2005, vol. 48, no. 21–22, pp. 4384–4396. DOI: 10.1016/ j.ijheatmasstransfer.2005.05.008

33. Schmidt, T., Assadi, H., Gärtner, F., Richter, H., Stoltenhoff, T., Kreye, H., & Klassen, T. From Particle Acceleration to Impact and Bonding in Cold Spraying. *Journal of Thermal Spray Technology*, 2009, vol. 18, no. 5–6, pp. 794–808. DOI: 10.1007/s11666-009-9357-7.

34. *Coldspray Meter: Research and industry standard for cold spray diagnostics*. Available at: https://spraysensors.tecnar.com/cold-spray/coldspray-meter/ (Last accessed: 04.05.2025).

ISSN 1814-4225 (print)
ISSN 2663-2012 (online)

Received 17.03.2025, Received in revised form 10.05.2025
Accepted date 17.11.2025, Published date 08.12.2025

МЕТОДОЛОГІЯ ВАЛІДАЦІЇ АНАЛІТИЧНИХ МОДЕЛЕЙ ДВОФАЗНИХ ПОТОКІВ У НАДЗВУКОВИХ СОПЛАХ З ВИКОРИСТАННЯМ CFD-МОДЕЛЮВАННЯ

О. В. Шорінов, С. О. Поливяний, Н. В. Савченко, Р. С. Іпатов

Предметом вивчення в статті є методологія математичного моделювання газодинамічних процесів у надзвукових звужувально-розширних соплах. **Метою** є розроблення та обґрунтування порівняльної методології валідації для оцінки точності спрощених аналітичних ізоентропійних моделей відносно високоточного CFD-моделювання для двофазних стисливих потоків із вторинним підсмоктуванням газу. **Завдання**: реалізувати чисельну модель течії газу з частинками всередині надзвукового сопла з використанням методу скінченних об'ємів (ANSYS Fluent); виконати аналітичні розрахунки швидкості та температури частинок з використанням одновимірної ізоентропійної моделі; провести порівняльний аналіз для виявлення систематичних відхилень та обґрунтування меж застосовності спрощеного аналітичного підходу порівняно з чисельним розв'язком. **Методи дослідження**: дослідження газодинаміки двофазного потоку виконано шляхом чисельного моделювання з використанням сучасного обчислювального пакету на основі методу скінченних об'ємів ANSYS Fluent, а також класичної газодинаміки. Були отримані наступні **результати**: чисельне моделювання двофазного потоку в соплі і одновимірна ізоентропійна модель були використані для аналізу поведінки частинок нікелю при різних температурах гальмування газу (440 °C, 520 °C і 620 °C) і діаметрах частинок (10 мкм, 25 мкм і 40 мкм). Результати CFD моделювання, які враховують реальну поведінку газу в каналі сопла, включаючи турбулентність, в'язкі ефекти і взаємодію частинок з потоком, були порівняні з аналітичними розрахунками. Результати CFD моделювання показують значно нижчі значення швидкості частинок (на 50 ± 7%) і вищі значення температури (на 22 ± 7%) порівняно з ізоентропійною моделлю, в першу чергу через врахування теплових втрат, розвитку примежового шару і впливу вторинної течії. Остання виникає внаслідок всмоктування потоку з частинками порошку з атмосфери в розширну частину сопла. Ці фактори порушують ідеальне розширення, прийняте в аналітичному підході, і зменшують розрахункові швидкість газу і частинок, одночасно підвищуючи температуру частинок. **Висновки.** Науковий внесок полягає в обґрунтуванні того, що класична ізоентропійна модель досягає межі своєї застосовності для сопел холодного напилення низького тиску з подачею порошку в надзвукову частину. Запропоновано введення поправочних коефіцієнтів, отриманих на основі CFD-даних, для уточнення аналітичних моделей. Практична значущість полягає у створенні основи для алгоритмів автоматизованого проєктування надзвукових сопел, що дозволяє виводити поправочні коефіцієнти для аналітичних рівнянь без необхідності проведення повторюваних ресурсоємних симуляцій у майбутньому.

Ключові слова: CFD моделювання; газовий потік; прискорення частинок; ANSYS Fluent; ізоентропійна модель.

Шорінов Олександр Володимирович – канд. техн. наук, доц., доц. каф. технології виробництва авіаційних двигунів, Національний аерокосмічний університет «Харківський авіаційний інститут», Харків, Україна.

Поливяний Сергій Олександрович – заступник директора з виробництва авіаційних двигунів – начальник виробничого управління АТ «Мотор Січ», Запоріжжя, Україна.

Савченко Ніна Валеріївна – канд. фіз.-мат. наук, доц., зав. каф. вищої математики та системного аналізу, Національний аерокосмічний університет «Харківський авіаційний інститут», Харків, Україна.

Іпатов Роман Сергійович – асп. каф. технології виробництва авіаційних двигунів, Національний аерокосмічний університет «Харківський авіаційний інститут», Харків, Україна.

Oleksandr Shorinov – Candidate of Technical Sciences, Associate Professor, Associate Professor at the Department of Aviation Engines Manufacturing Technology, National Aerospace University «Kharkiv Aviation Institute», Kharkiv, Ukraine,
e-mail: o.shorinov@khai.edu, ORCID: 0000-0002-5057-6679, Scopus Author ID: 57223082183.

Sergii Polyviany – Deputy Director for Manufacturing of Aviation Engines – Head of Manufacturing Department at JSC «Motor Sich», Zaporizhzhia, Ukraine,
e-mail: sergeypolyvanij@ukr.net, ORCID: 0000-0003-0558-1353, Scopus Author ID: 57224730128.

Nina Savchenko – Candidate of Physical and Mathematical Sciences, Associate Professor, Head of the Department of Higher Mathematics and System Analysis, National Aerospace University «Kharkiv Aviation Institute», Kharkiv, Ukraine,
e-mail: n.savchenko@khai.edu, ORCID: 0000-0001-8144-9368, SCOPUS Author ID: 56421771100.

Roman Ipatov – PhD Student of the Department of Aviation Engines Manufacturing Technology of National Aerospace University «Kharkiv Aviation Institute», Kharkiv, Ukraine,
e-mail: r.s.ipatov@khai.edu, ORCID: 0009-0007-3620-7897.